JOURNAL OF GEOPHYSICAL RESEARCH: PLANETS, VOL. 118, 278–291, doi:10.1002/jgre.20053, 2013

Distribution of Early, Middle, and Late Noachian cratered surfaces in the Martian highlands: Implications for resurfacing events and processes

Rossman P. Irwin III,[1] Kenneth L. Tanaka,[2] and Stuart J. Robbins[3]

Received 4 October 2012; revised 16 January 2013; accepted 18 January 2013; published 25 February 2013.

[1] Most of the geomorphic changes on Mars occurred during the Noachian Period, when the rates of impact crater degradation and valley network incision were highest. Fluvial erosion around the Noachian/Hesperian transition is better constrained than the longer-term landscape evolution throughout the Noachian Period, when the highland intercrater geomorphic surfaces developed. We interpret highland resurfacing events and processes using a new global geologic map of Mars (at 1:20,000,000 scale), a crater data set that is complete down to 1 km in diameter, and Mars Orbiter Laser Altimeter topography. The Early Noachian highland (eNh) unit is nearly saturated with craters of 32–128 km diameter, the Middle Noachian highland (mNh) unit has a resurfacing age of ~4 Ga, and the Late Noachian highland unit (lNh) includes younger composite surfaces of basin fill and partially buried cratered terrain. These units have statistically distinct ages, and their distribution varies with elevation. The eNh unit is concentrated in the high-standing Hellas basin annulus and in highland terrain that was thinly mantled by basin ejecta near 180° longitude. The mNh unit includes most of Arabia Terra, the Argyre vicinity, highland plateau areas between eNh outcrops, and the Thaumasia range. The lNh unit mostly occurs within highland basins. Crater depth/diameter ratios do not vary strongly between the eNh and mNh units, although crater losses to Noachian resurfacing appear greater in lower lying areas. Noachian resurfacing was spatially non-uniform, long-lived, and gravity-driven, more consistent with arid-zone fluvial and aeolian erosion and volcanism than with air fall mantling or mass wasting.

Citation: Irwin, R. P., III, K. L. Tanaka, and S. J. Robbins (2013), Distribution of Early, Middle, and Late Noachian cratered surfaces in the Martian highlands: Implications for resurfacing events and processes, *J. Geophys. Res. Planets*, *118*, 278–291, doi:10.1002/jgre.20053.

1. Introduction

[2] The cratered highland geologic province of Mars is remarkable for its abundant degraded impact craters and fluvial landforms, which are rare to absent on younger surfaces [e.g., *Carr*, 1995; *Hynek et al*., 2010]. Relict impact craters dating to the Noachian Period (>3.57–3.74 Ga) [*Hartmann and Neukum*, 2001; *Hartmann*, 2005; *Werner and Tanaka*, 2011] have reworked ejecta blankets, reduced rims, gullied interior walls, low-gradient to flat floors, and partly to wholly buried central peaks [e.g., *Arvidson*, 1974; *Craddock and Maxwell*, 1993; *Forsberg-Taylor et al*., 2004]. Modeling of equatorial crater degradation by fluvial, aeolian, and mass-wasting processes suggests a dominant fluvial signature, but with contributions from other processes [*Craddock et al*., 1997; *Forsberg-Taylor et al*., 2004; *Howard*, 2007; *Mangold et al*., 2012a]. Some craters contain predominantly volcanic [e.g., *Arvidson et al*., 2006; *Fassett and Head*, 2008a] or aeolian fill materials [e.g., *Grant and Schultz*, 1993; *Barlow*, 1995; *Edgett*, 2005; *Lewis et al*., 2008]. Crater modification at higher latitudes included post-Noachian, ice-facilitated mass wasting and mantling [e.g., *Jankowski and Squyres*, 1992, 1993; *Berman et al*., 2009].

[3] Most counts of impact craters superimposed on valley networks record a timing of dissection around the Noachian/Hesperian transition, although some fluvial activity appears to have occurred later [e.g., *Gulick and Baker*, 1990; *Irwin and Howard*, 2002; *Mangold et al*., 2004, 2012b; *Fassett and Head*, 2008b; *Bouley et al*., 2009; *Hoke and Hynek*, 2009]. Large alluvial fans and deltas, many of which have well-preserved distributary channel networks in inverted relief, may date to the Late Hesperian or Early Amazonian Epochs [*Grant and Wilson*, 2011; *Mangold et al*., 2012b; *Irwin and Grant*, 2013].

[1]Center for Earth and Planetary Studies, National Air and Space Museum, Smithsonian Institution, Washington, D.C., USA.
[2]U. S. Geological Survey, Astrogeology Science Center, Flagstaff, Arizona, USA.
[3]Laboratory for Atmospheric and Space Physics, University of Colorado, Boulder, Colorado, USA.

Corresponding author: R. P. Irwin III, Center for Earth and Planetary Studies, National Air and Space Museum, Smithsonian Institution, MRC 315, 6th St. at Independence Ave. SW, Washington, D.C. 20013, USA. (irwinr@si.edu)

2169-9097/13/10.1002/jgre.20053

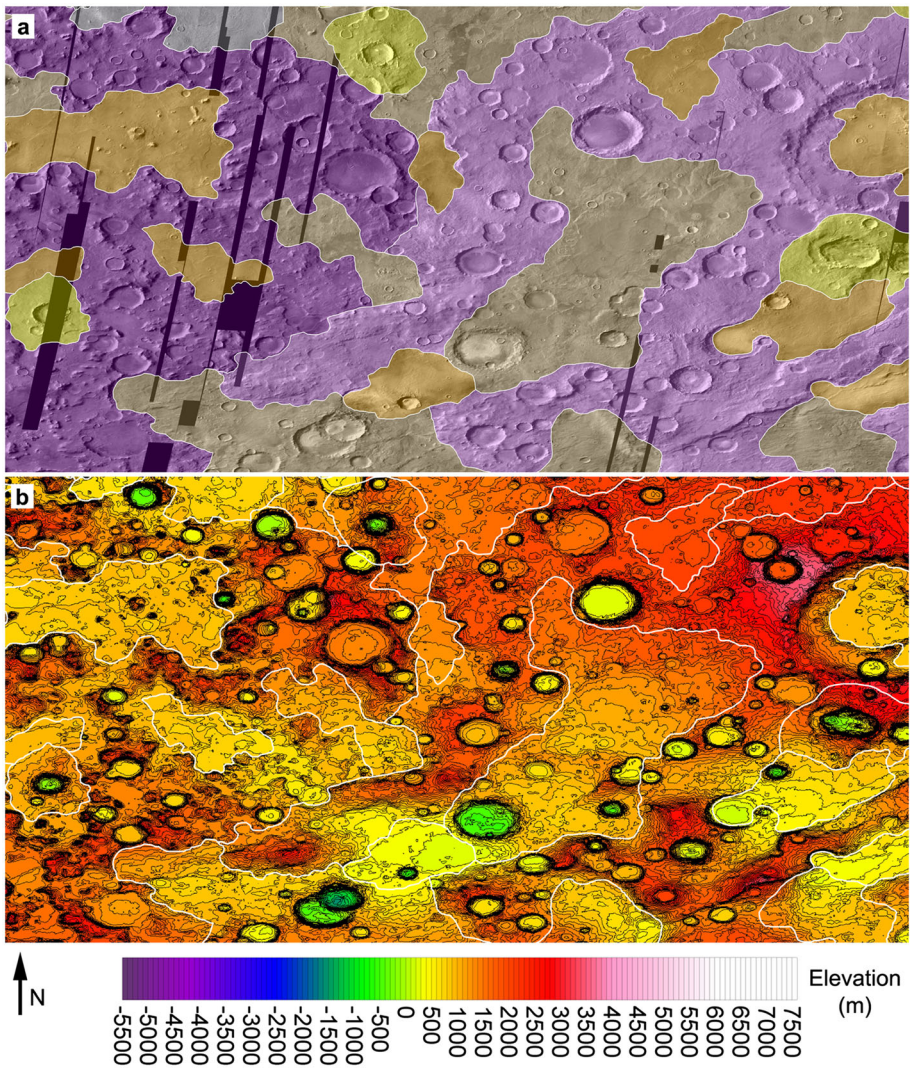

Figure 1. (a) Example of contact relationships between the impact (yellow), Late Noachian highland (orange), Middle Noachian highland (tan), Early Noachian highland (light purple), and Early Noachian highland massif (dark purple) units (legend as in Figure 2). Contact attribution as certain or approximate is not shown. (b) The same scene in MOLA 64 pixel/degree topography, contoured at 100 m intervals. Cylindrical projection centered at 49.5°S, 128°E, 1080 km across at the center.

[4] Many workers have noted the broad, undissected interfluvial surfaces and low drainage density of Martian valley networks [e.g., *Pieri*, 1980; *Mars Channel Working Group*, 1983; *Carr and Chuang*, 1997], suggesting that the valleys dissect an older geomorphic surface. This surface has received relatively little attention in the literature [e.g., *Malin*, 1976; *Grant*, 1987], although its development reflects geomorphic processes and environmental conditions that span much of the Noachian Period. In contrast, the incision of valley networks appears to represent one or more geologically brief intervals of time [*Howard et al.*, 2005; *Irwin et al.*, 2005; *Fassett and Head*, 2008b; *Barnhart et al.*, 2009; *Grant and Wilson*, 2011; *Mangold et al.*, 2012b]. Improved characterization of pre-valley resurfacing events and processes in the highlands would provide better insight into long-term conditions, which are more relevant to habitability than are shorter-lived valley networks.

[5] The purpose of this study is to determine whether Noachian highland resurfacing was spatially uniform, or if it depended on topography or proximity to large impact basins. Answering these questions will help to constrain the major highland resurfacing events and processes prior to valley network incision. We use geologic unit boundaries from a new global geologic map of Mars at 1:20,000,000 scale (K. L. *Tanaka et al.*, Global geologic map of Mars, manuscript in review, 2012, hereinafter referred to as *Tanaka et al.*, in review); a database of crater location, depth, and diameter from *Robbins and Hynek* [2012a, 2012b]; and gridded topographic data from the Mars Global Surveyor Mars Orbiter Laser Altimeter (MOLA) [*Smith et al.*, 2001; *Neumann et al.*, 2004]. This study tests four null hypotheses pertaining to the Early Noachian highland (eNh), Middle Noachian highland (mNh), and Late Noachian highland (lNh) geologic units identified in the global geologic map (Figure 1):

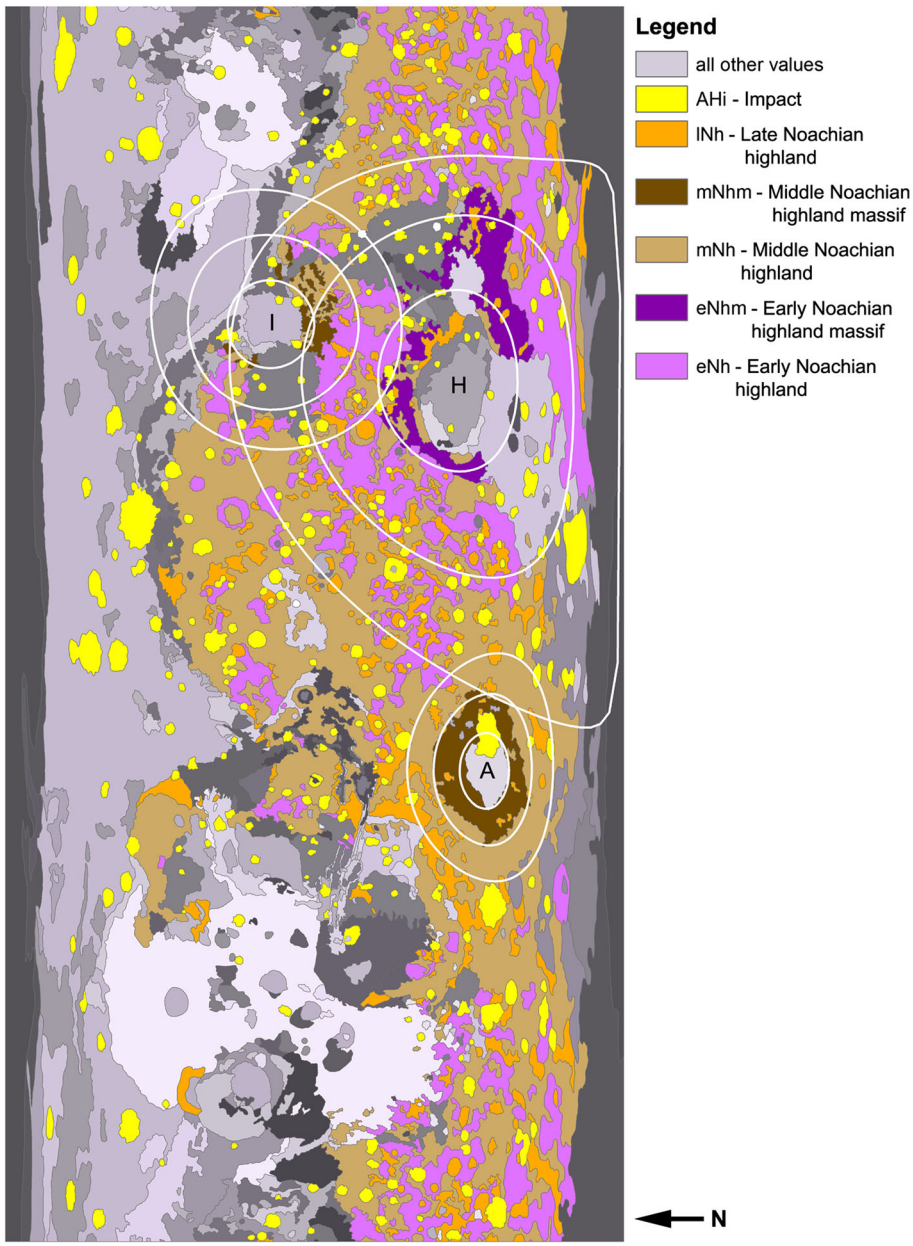

Figure 2. Global geologic map of Mars (90°N–90°S, 180°W–180°E) (*Tanaka et al.*, in review), with Noachian and impact units of interest in this study highlighted. All other units are shown in gray tones. Also shown are the expected zones of greatest resurfacing from Hellas, Isidis, and Argyre basin ejecta, which would be within one basin diameter of the inner basin ring. Multiples of 1, 2, and 3 inner basin ring radii are shown with white lines. Note the concentration of the eNh unit within the Hellas basin annulus.

(1) The eNh, mNh, and lNh units have statistically indistinguishable crater densities;
(2) The eNh and mNh crater depth/diameter ratios are drawn from the same probability distribution;
(3) The spatial distribution of eNh, mNh, and lNh units is independent of topography; and
(4) The visible crater density is independent of proximity to the Hellas, Isidis, and Argyre impact basins.

[6] Hypothesis 1 addresses the validity of the three geologic units, which are defined by age in the global geologic map, although their contacts are based on morphology as seen in imaging and topographic data (the map units and mapping methodology are described in section 2.1 below). If the eNh, mNh, and lNh unit crater populations follow a production function above 32 km in diameter (an erosional roll-off is expected below ~32 km [e.g., *Hartmann*, 1966; *Chapman and Jones*, 1977]), and the error bars in larger-diameter bins of older units generally do not intersect those of younger units, then the three mapped units have distinct ages. We would reject the null hypothesis and conclude that the units experienced resurfacing at different times and/or rates. Alternatively, if for example the mapped eNh outcrops are simply clusters of larger craters sampled from a younger, more

extensive geologic unit, then the eNh and mNh crater populations would not follow a production function above 32 km.

[7] Hypothesis 2 focuses on crater depth/diameter ratios, which should be lower on average for older geologic units, if Noachian crater degradation and resurfacing were spatially and temporally uniform. Alternatively, if the mNh unit has crater depth/diameter ratios that are indistinguishable from or lower than those of eNh, with relative ages established under Hypothesis 1, then crater infilling must have been more rapid in the mNh unit. The lNh unit is mostly basin fill, and its visible craters are either fresh, deeply buried, or small outcrops of older incorporated materials, so this test is not meaningful for that unit. We also limit this hypothesis test to $\pm 30^\circ$ latitudes, as craters at higher latitudes have experienced significant post-Noachian infilling and periglacial degradation [e.g., *Jankowski and Squyres*, 1992, 1993; *Robbins and Hynek*, 2012b]. We do not expect this later modification to have significantly reduced crater densities >32 km in diameter [e.g., *Soderblom et al.*, 1974], so a latitudinal constraint is not needed for Hypothesis 1. Hypotheses 3 and 4 evaluate possible causes for any differences in Noachian crater degradation and loss.

[8] Hypothesis 3 addresses topographic relationships between the eNh, mNh, and lNh units. If the eNh unit is shown to occupy higher elevations, as was observed during mapping, then resurfacing was topographically concentrated at lower elevations. On a local spatial scale, more resurfacing at lower elevations would be expected from volcanism or fluvial erosion, whereas air fall mantling deposits should be less sharply constrained by topography. At a regional scale, preferential resurfacing at lower elevations may reflect a resurfacing event that was limited to a low-lying cratered region.

[9] Hypothesis 4 evaluates a possible resurfacing signature from the Hellas, Isidis, and Argyre basin impacts in the crater populations. These impacts had the potential to reset crater populations on surfaces within at least one inner-ring diameter of the inner basin ring (although some larger buried craters may retain some topographic expression). Determining the ages of these impacts [e.g., *Werner*, 2008; *Fassett and Head*, 2011; *Robbins and Hynek*, 2012c] and the extent of their ejecta will help to evaluate their possible role in landscape resurfacing, relative to erosional and volcanic processes.

[10] Testing these hypotheses collectively provides some insight into whether and why Noachian resurfacing was spatially focused. None of these methods makes a unique link to specific geomorphic processes, aside from resurfacing by impact basin ejecta, but establishing topographic control on highland resurfacing would exclude processes that are expected to be more spatially uniform, such as air fall mantling. Fluvial erosion and flood volcanism are expected to primarily infill lower lying surfaces, although running water would also degrade the surrounding slopes, making it more consistent with erosion and infilling across a wide range of elevations.

2. Methods

2.1. Geologic Mapping

[11] The geologic unit boundaries for this study are taken from the draft 1:20,000,000-scale global geologic map of Mars (Figure 2). Tanaka et al. (in review) drafted the line work at 1:5,000,000 scale on a base combining the MOLA digital elevation model (128 pixels/degree, or ~463 m/pixel at the equator) and the Mars Odyssey Thermal Emission Imaging System (THEMIS) daytime infrared (DIR) base image mosaic, which is sampled at 100 m/pixel. Line work was stream-digitized with a standard vertex spacing of 5 km, and nodes were snapped to form continuous polygons. Unit contacts were attributed as certain or approximate. Outcrop areas used for crater density determinations were derived in ArcGIS by calculating areas as defined on a sphere in geographic (unprojected) coordinates.

[12] Six contacts are most relevant to this study. First, the contact between the eNh and mNh units was typically defined at a break in slope between a more steeply sloping, higher-standing, heavily cratered surface (unit eNh) and a more gently sloping, less densely cratered surface below it (unit mNh). At sharp slope breaks, such as the base of a well-defined escarpment, the contact was often attributed as certain, whereas concave breaks in slope more commonly received approximate contacts. The mNh unit has a higher density of degraded impact craters and steeper slopes when compared to the lNh unit, which is mostly younger basin fill. Second, the nearly flat-lying lNh outcrops typically have certain contacts with eNh or mNh outcrops. The lNh unit does contain some degraded impact craters, which distinguish it from the Early Hesperian highland (eHh) unit that contains generally fresh-appearing craters on flat, low-lying surfaces. The third contact is between Hesperian or Amazonian units and older units. These contacts are usually sharply defined, mapped as certain, and interpreted as the margin of volcanic or other plains materials.

[13] The fourth contact is the margin of fresh crater ejecta (Amazonian-Hesperian impact unit, AHi) with surrounding materials. These contacts are frequently located at the margin of the continuous ejecta, and they are labeled approximate where discontinuous ejecta extend beyond the contact or where continuous margins are not well defined.

[14] The Early Noachian highland massif (eNhm) and Middle Noachian highland massif (mNhm) unit contacts surround rugged, mountainous areas near large impact basins. These two contacts include significant portions of both certain and approximate contacts with eNh and mNh outcrops and mostly certain contacts with younger lNh and other units. The contacts with units of similar age are based on both topographic slope breaks and morphologic changes that can be sharp or gradual.

2.2. Crater Counts

[15] This study utilized the Martian impact crater database of *Robbins and Hynek* [2012a, 2012b], which contains 384,335 craters and is complete down to 1 km in diameter. Craters were identified and measured manually using THEMIS DIR global mosaics, which were searched several times to ensure as complete a count as possible. MOLA gridded topography was also searched for craters that had a topographic expression but no obvious visible one. The complete catalog contains nearly 640,000 craters down to diameters (D) as small as ~0.5 km to ensure a statistical completeness globally to $D \geq 1$ km [see *Robbins and Hynek*, 2012a, section 2).

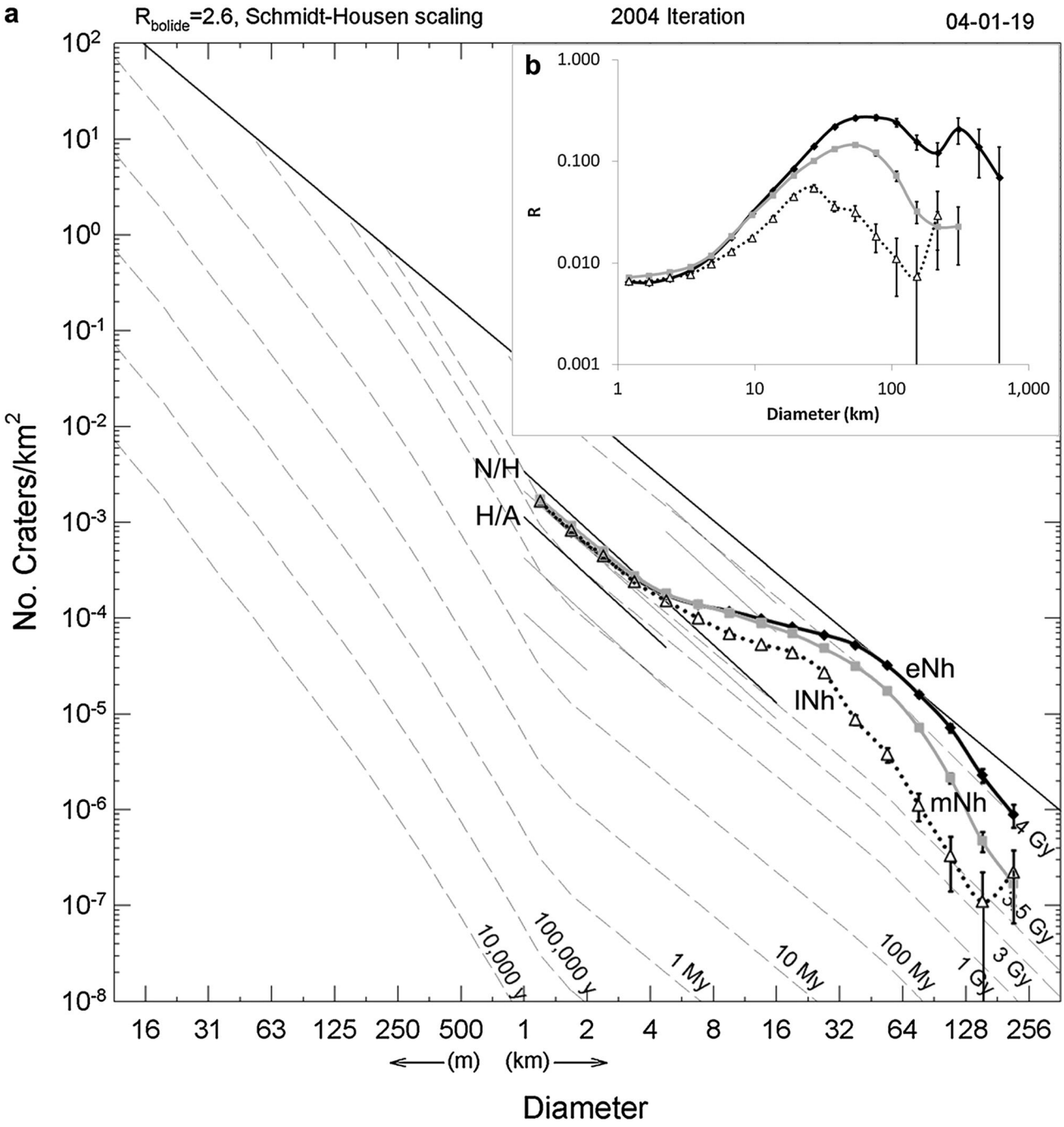

Figure 3. (a) Crater counts from the *Robbins and Hynek* [2012a, 2012b] database for the eNh (black line), mNh (gray line), and lNh (dotted line) units, superimposed on the isochron plot from *Hartmann* [2005]. The Noachian/Hesperian (N/H) and Hesperian/Amazonian (H/A) boundaries defined by *Tanaka* [1986] are labeled. Straight, solid gray lines are epoch boundaries within those periods. Crater counts include fresh and degraded craters assigned to units as discussed in the text. Error bars are shown but are smaller than the point symbols for most diameter bins. The units have statistically distinct ages. (b) Relative plot of the same data, where $R = N\bar{D}^{-3}/[A(D_b - D_a)]$, N is the number of craters in each bin, the bin diameter range is D_a to D_b (km), $\bar{D}$ is the geometric mean of crater diameters in the bin (km, approximated by $D = (D_b D_a)^{0.5}$), and A is the counting area (km^2).

[16] We loaded the crater database into ESRI ArcGIS 9.3 software as a point shapefile. Underlying layers included a polygon shapefile of the draft global geologic map, the 256 pixel/degree THEMIS DIR mosaic, and topographic contour maps derived from the 64 pixel/degree MOLA Mission Experiment Gridded Data Record (MEGDR). We selected crater points by location intersecting the eNh, mNh, and lNh units, producing three raw crater point shapefiles associated with these units. These raw shapefiles required editing to add large fresh craters and to reassign some older

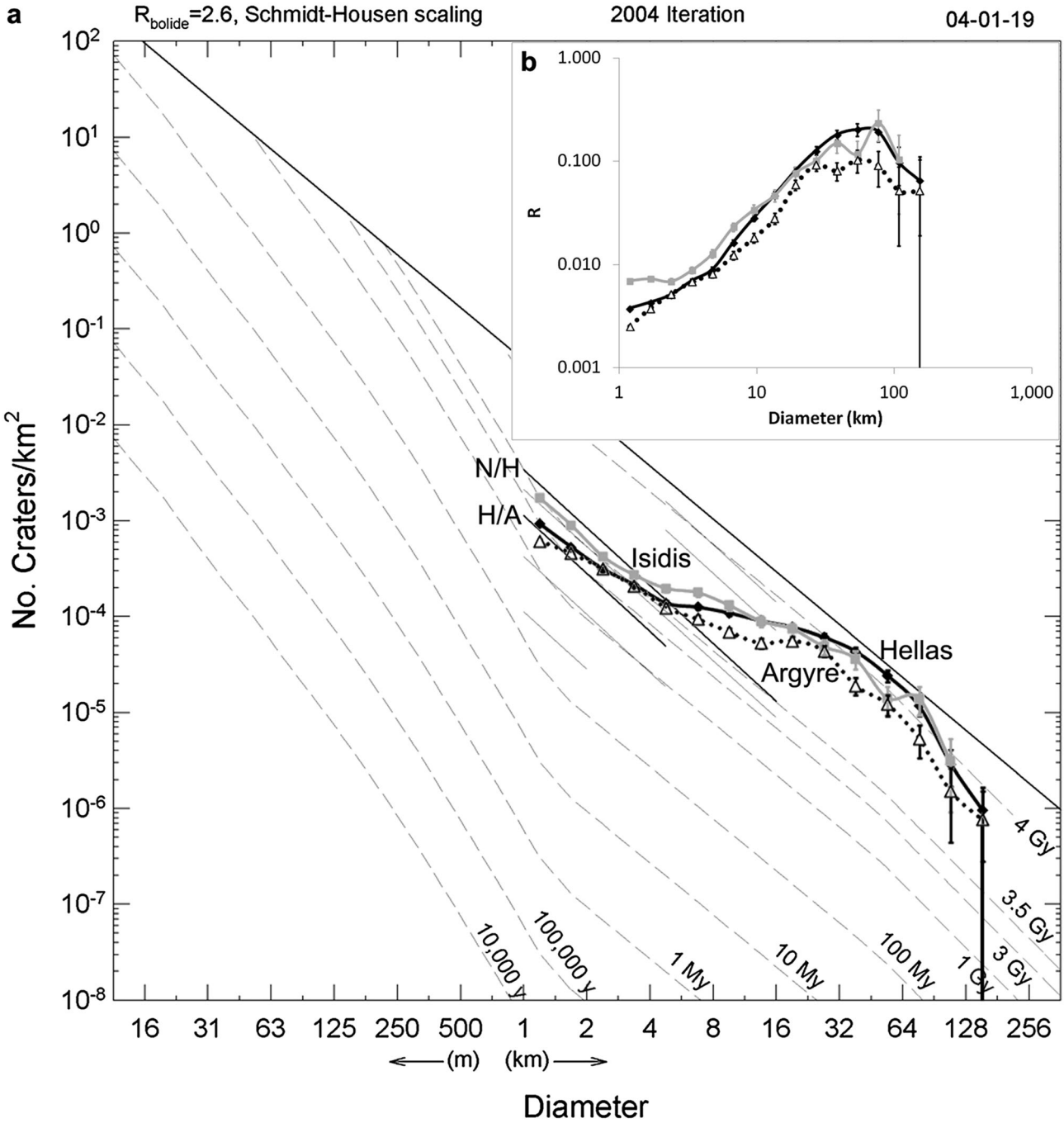

Figure 4. (a) Crater counts from the *Robbins and Hynek* [2012a, 2012b] database for the eNhm Hellas (black line), mNhm Isidis (gray line), and mNhm Argyre (dotted line) units, superimposed on the isochron plot from *Hartmann* [2005]. The unit areas were 2,039,461; 632,465; and 1,285,540 km^2; respectively, inclusive of superimposed AHi outcrops. The Noachian/Hesperian (N/H) and Hesperian/Amazonian (H/A) boundaries defined by *Tanaka* [1986] are labeled. Straight, solid gray lines are epoch boundaries within those periods. Crater counts include fresh and degraded craters assigned to units as discussed in the text. Error bars are shown but are smaller than the point symbols for most diameter bins. (b) Relative plot of the same data, as described in Figure 3b.

craters whose rim and floor fell within different geologic units, as described below.

[17] Craters in the 1–4 km diameter bins for all three units followed the same *Hartmann* [2005] isochron line with a mid-Hesperian age of about 3.5 Ga, whereas those in the 4–32 km bins showed resurfacing losses inverse to diameter (alternatively, much of this slope may result from a distinct production population during heavy bombardment [e.g., *Strom et al.*, 1992]), and craters of 32–128 km for the eNh and mNh units followed separate Noachian Hartmann isochron lines. The mid-Hesperian production population from 1 to 4 km suggests a complete post-Noachian resurfacing

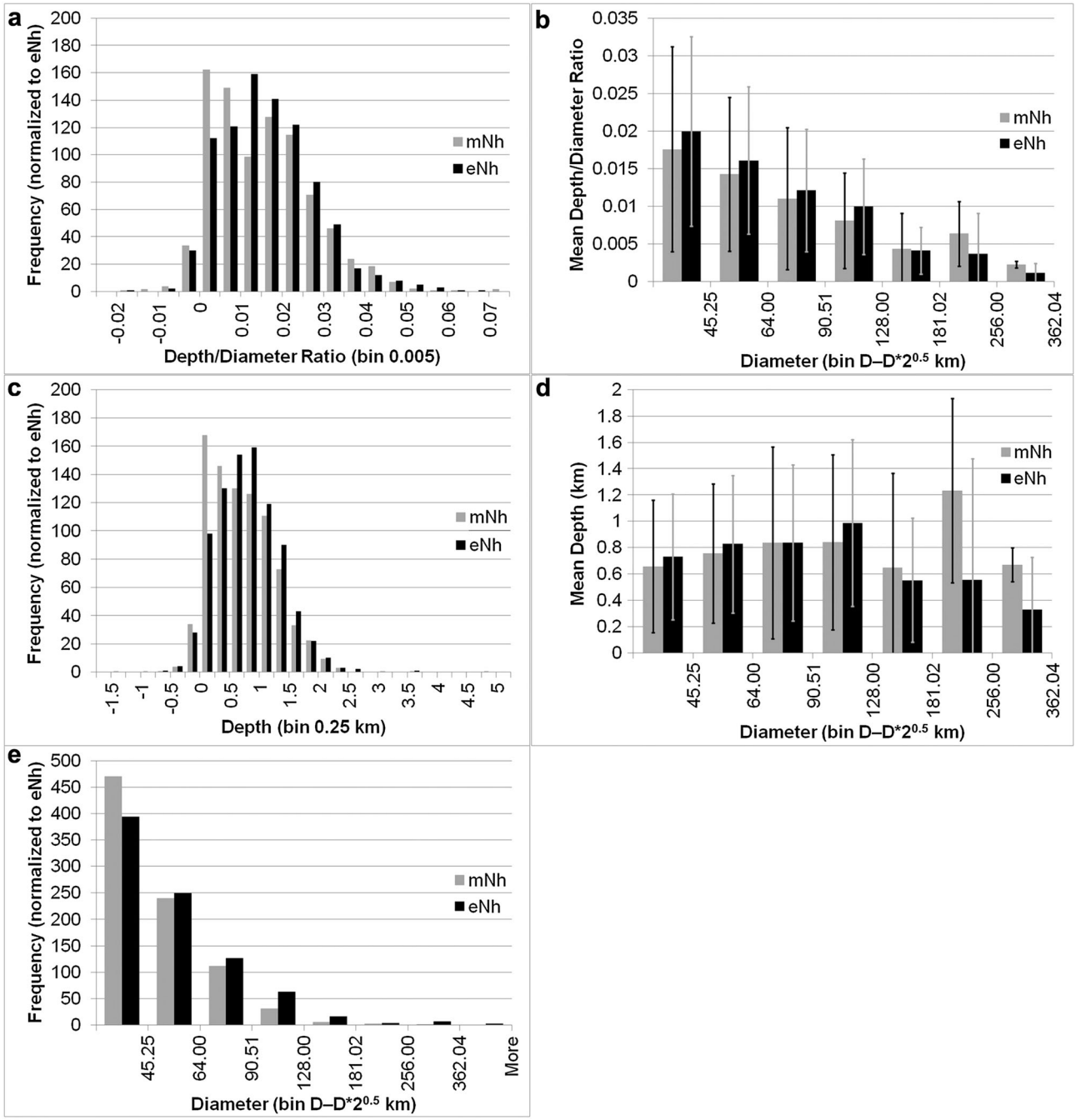

Figure 5. Depth and diameter relationships for impact craters >32 km in diameter in the eNh and mNh units. (a) Histogram of depth/diameter ratio, with the mNh unit frequency normalized to the total number of craters in the eNh unit (there were 1123 craters in mNh and 864 in eNh in this diameter range). (b) Mean depth/diameter ratio and standard deviation for craters in the diameter bins shown. We found no statistically significant difference in depth/diameter ratios of craters between the eNh and mNh units. (c) Histogram of crater depth, normalized similarly to Figure 5a. Note the relative abundance of shallow craters in the mNh unit. Negative depths are possible where the surface outside a crater is deeply denuded or the interior is filled above the rim. (d) Mean depth and standard deviation for craters in the diameter bins shown. We found no statistically significant relationship between depth and diameter for all craters or by unit. The 181–256 km bin contains three craters and is heavily influenced by the deep craters Baldet and Mutch. (e) Histogram of crater diameter, normalized similarly to Figure 5a.

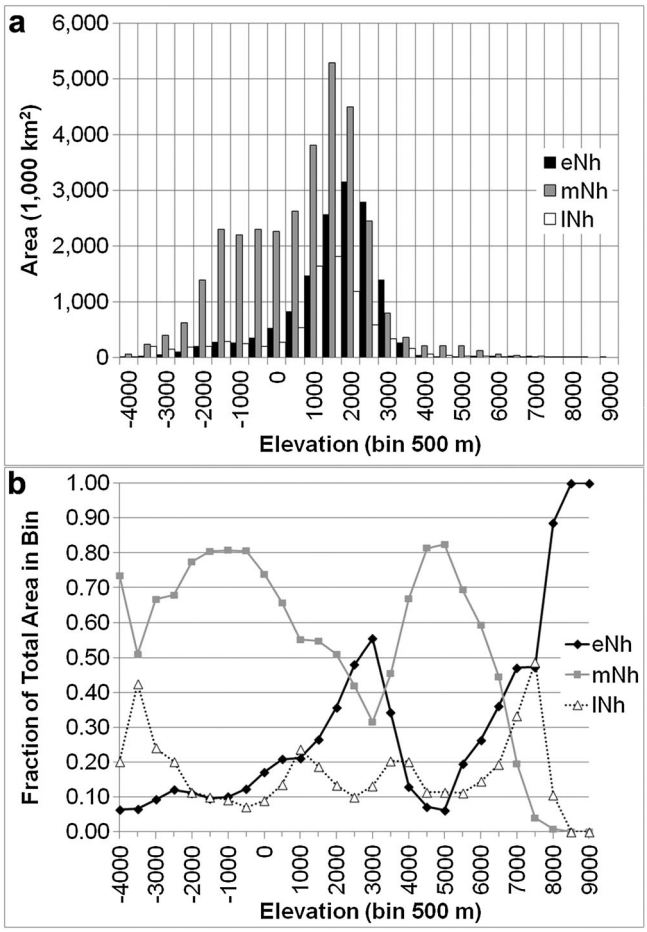

Figure 6. (a) Elevation histogram showing the total area of each unit in 500 m elevation bins. The shoulder in the mNh unit is Arabia Terra at −2000 to +500 m. (b) Plot of the fractional area of each geologic unit in each 500 m elevation bin. Major features are driven by Arabia Terra from −2000 to +500 m, the highland plateau from 500 to 2000 m, the Hellas annulus where eNh is dominant between 2000 and 3000 m, and the Thaumasia range above 3000 m.

of the highlands on that spatial scale, so craters in that diameter range cannot be used to date Noachian resurfacing events [e.g., *Barlow*, 1988]. To determine a relative age for the last complete resurfacing of each Noachian unit, we primarily used craters >32 km in diameter.

[18] In the geologic map, morphologically fresh impact craters and their visible ejecta blankets were mapped as a separate Amazonian to Hesperian impact unit, AHi. Each outcrop polygon in the global geologic map is at least 100 km long and 40 km wide, and impact craters in the 32–45.25 km and larger diameter bins may have ejecta blankets >100 km wide, so those craters are typically isolated in the AHi unit from the Noachian geologic units that they overlie. We added a column to the AHi unit attribute table in ArcGIS and assigned an underlying geologic unit for each AHi polygon, based on inspection of the map, THEMIS base mosaic, and MOLA topography. This procedure allowed us to add the area and crater populations of the AHi outcrops to the underlying units. The ejecta blankets of large fresh craters typically have lower densities of small craters relative to the subjacent Noachian units, but the area resurfaced by the ejecta of large craters is relatively small (6% of the total area of eNh plus superimposed AHi, or 7% for mNh and lNh), so it has little effect on the combined (highland plus impact unit) small-crater densities.

[19] Another issue in the global map is that many large degraded craters have their rim in an older unit and their floor and center point in a younger one, due to partial burial or embayment. The consequence is that in larger diameter bins, the lNh unit would appear older than it actually is, whereas the mNh and eNh units would appear somewhat younger than their age. We inspected all 421 craters of >32 km diameter whose centers fell within the lNh unit, and we classified them as superimposed, buried, or partly buried with a substantial portion of their rim in the eNh or mNh units. We followed the same procedure for craters >32 km diameter in the mNh unit. Where parts of a crater rim crosscut both the eNh and mNh units, as opposed to cutting eNh and being embayed by mNh, it was assigned to the younger unit. For smaller embayed craters of >32 km diameter that included a contact, we interpreted which unit would have contained the crater center prior to the impact. This procedure added craters to older units without adding area, which may lead to a slight overestimation of age.

2.3. Data Analysis

[20] We determined the relative age of each unit by dividing its crater data into diameter bins of $D - D*2^{0.5}$ km, with both the count (N) and error bars ($\pm N^{0.5}$) normalized to an area of 10^6 km^2 [e.g., *Hartmann*, 2005]. As previous workers have noted, diameter bins below about 32 km have reduced crater densities due entirely or in part to resurfacing that did not destroy the larger-diameter craters [e.g., *Öpik*, 1966; *Hartmann*, 1966; *Chapman et al*., 1969; *Soderblom et al*., 1974; *Chapman and Jones*, 1977; *Strom et al*., 2005], so we used the >32 km bins as our main method for unit age determination. The cause of the roll-off in crater populations below 32 km has been controversial, with studies advocating either preferential resurfacing at smaller diameters, changes in the crater production function with time, or some combination [e.g., *Oberbeck et al*., 1977; *Barlow*, 1988, 1990; *Strom et al*., 1992, 2005]. In this context, we note that secondary craters are preserved mainly around large craters that postdate the most significant valley network incision around the Noachian/Hesperian transition, so craters in the size range of secondaries (at a minimum) were eradicated along with the severe morphological degradation and burial that is observed for larger Noachian craters. This observation is consistent with the mid-Hesperian production population from 1 to 4 km in diameter in the highlands. We plotted the binned data on the *Hartmann* [2005] isochron chart and on a relative chart (Figures 3 and 4) [*Crater Analysis Techniques Working Group*, 1979]. The *Hartmann* [2005] model absolute ages differ little from Neukum's work during the Noachian Period [e.g., *Hartmann and Neukum*, 2001; *Ivanov*, 2001; *Werner and Tanaka*, 2011], and the relative rather than absolute ages are the focus here. However, the crater densities for all three units at $D > 90$ to $D > 128$ km are significantly less than the *Hartmann* [2005] isochrons would predict, based on densities at 32–90 km diameter. Lower than expected densities of large craters are likely not attributable to preferential resurfacing at

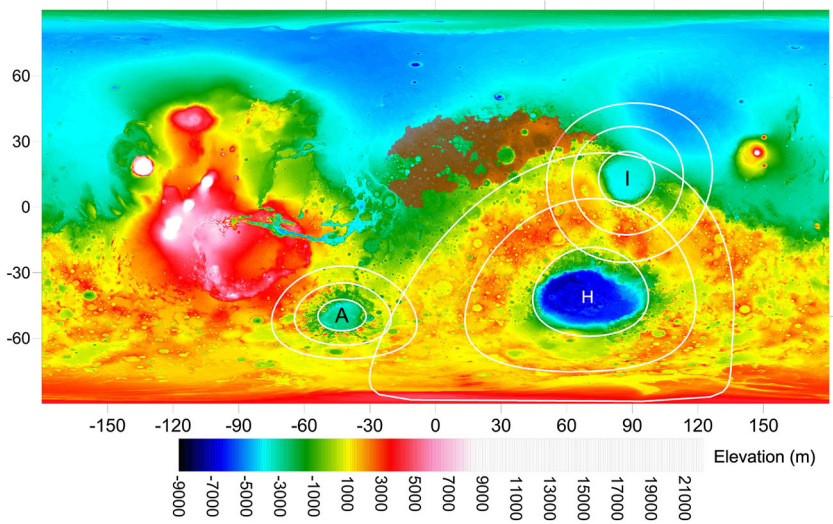

Figure 7. MOLA MEGDR global topography (16 pixels/degree) showing expected zones of greatest resurfacing from Hellas (H), Isidis (I), and Argyre (A) basin ejecta, which would be deposited within one basin diameter of the inner basin ring. Multiples of 1, 2, and 3 inner basin ring radii are shown with white lines. Note the concentration of high-standing topography within the Hellas basin annulus [*Smith et al.*, 2001]. The Arabia Terra crater count area (Table 1) is highlighted in red, northwest of the Hellas annulus. The Arabia region experienced extensive Middle Noachian resurfacing mostly beyond the thickest basin ejecta blankets.

Table 1. N(16) Relative Ages of Geologic Units

Unit[a]	N(16)	Epoch(s)[b]
Late Noachian highland (lNh)	85 ± 3	Late Noachian
Middle Noachian highland massif, Argyre (mNhm)	141 ± 10	Middle Noachian
Middle Noachian highland (mNh)	179 ± 2	Middle Noachian
Middle Noachian highland, Arabia (subset of mNh)	186 ± 6	Middle Noachian
Middle Noachian highland massif, Isidis (mNhm)	191 ± 17	Early or Middle Noachian
Early Noachian highland massif, Hellas (eNhm)	223 ± 10	Early Noachian
Early Noachian highland (eNh)	262 ± 4	Early Noachian

[a]Includes superimposed fresh craters from the impact unit, AHi.
[b]Following the *Werner and Tanaka* [2011] scheme.

large diameters, so a change in the production function with time may be responsible for the discrepancy [e.g., *Barlow*, 1988, 1990; *Strom et al.*, 1992, 2005].

[21] We examined the depth and diameter of all craters >32 km in diameter, as assigned to geologic units in the manner described above, within the ±30° latitude range (Figure 5). For depth, we used the exterior surface minus floor elevations as described by *Robbins and Hynek* [2012a]. We used a single-factor analysis of variance (ANOVA) to test the hypothesis that the eNh and mNh units' depth, diameter, and depth/diameter ratio data were drawn from the same underlying probability distributions. Histograms of the depth, diameter, and depth/diameter ratios are provided in Figure 5.

[22] We evaluated the topographic distribution of the eNh, mNh, and lNh units by saving the 8 pixel/degree MOLA MEGDR as a *X-Y-Z* coordinate, comma-delimited text file, importing it into ArcGIS as a point shapefile, and selecting points that intersected (were contained within) the polygons of each unit. We calculated the area of each grid cell as a function of latitude and binned the area data in 500 m elevation increments. These data are shown as elevation histograms in Figure 6a. We then compared the fraction of each elevation bin that fell within each unit (Figure 6b). This elevation analysis does not include superimposed fresh craters from unit AHi.

[23] Finally, we dated the Hellas, Isidis, and Argyre impact basins using crater counts on their respective highland massif unit polygons. These units contain the rugged, mountainous surfaces that are related to impact basin formation. We also examined the area within one inner ring diameter of the inner basin ring, which should contain the thickest ejecta deposits, to see whether the eNh unit was exposed in the area (Figures 2 and 7). If both the highland massif unit and the surroundings were Middle Noachian surfaces, as is the case with Argyre, then the basin was assigned a Middle Noachian age. Alternatively, if the highland massif unit was Early Noachian, and the surroundings contained eNh outcrops, then the basin was assigned an Early Noachian age, as with Hellas. These two large impact basins and Isidis may have formed secondary craters up to several tens of kilometers in diameter outside the area of

the thickest basin ejecta deposits [*Melosh*, 1989], whereas the highland massif units are located within that area and should have little contamination by secondaries. The area surrounding these large impact basins may also contain craters buried by basin ejecta, as the *Robbins and Hynek* [2012a, 2012b] database does contain buried craters. For these reasons, our best age estimates should come from the highland massif units rather than from outlying surfaces.

3. Results

3.1. Hypothesis 1: Impact Crater Densities

[24] The null hypothesis for this analysis is that the eNh, mNh, and lNh units have statistically indistinguishable crater densities. The crater counts in Figure 3 show that the units have distinct ages well outside the error bars for each diameter bin >32 km, and the N(16) ages in Table 1 have the same relationships, so the null hypothesis is rejected. Figure 3 shows that the eNh unit approaches saturation at diameters of 32–128 km, with a reduction between 4 and 32 km and a mid-Hesperian (~3.5 Ga) production population from 1 to 4 km. The mNh crater population follows a similar pattern from 1 to 4 and from 4 to 32 km, but the age defined by the 32–128 km bins approximately follows *Hartmann*'s [2005] 4 Ga isochron line. The lNh unit also has a production population between 1 and 4 km, but the edited data set does not maintain a production population for $D > 32$ km.

[25] To recognize the effect of reassigning craters from lNh and mNh to older units, as described above, we compared the edited crater counts to the raw ones (not shown), which were derived from a simple selection of the unit on which the crater center was located. The raw counts gave essentially the same age result for the eNh and mNh units in bins up to 128 km, and there was only a slight age reduction in the raw counts for the 128–256 km bins, but not enough to change the geologic epoch. The lNh unit was mapped as highland basin fill, but the resurfacing was incomplete in places, and some degraded craters are included. The unit is therefore a composite surface including mostly Late Noachian degraded craters and various basin fill materials of Late Noachian to perhaps Early Hesperian age. Meaningful subdivision of these materials was not possible at the 1:20,000,000 map scale.

[26] These results show that (1) a recognizable, extensive geologic unit (eNh) is nearly saturated with impact craters at 32–128 km diameters; (2) a more extensive geologic unit (mNh) is undersaturated, with a model absolute age of about 4 Ga; and (3) a composite surface of basin fill materials and some impact craters (lNh) reflects later resurfacing in localized areas. Taken together, these results show that loss of impact craters to burial or erosion was not spatially uniform on Noachian Mars.

3.2. Hypothesis 2: Impact Crater Depth/Diameter Ratios

[27] Hypothesis 2 is that the eNh and mNh crater depth/diameter ratios are drawn from the same probability distribution. If crater degradation were spatially and temporally uniform throughout the duration of the visible cratering record, then the average crater should be shallower relative to its diameter on older, more densely cratered surfaces. Alternatively, if craters were more likely to remain enclosed on high-standing surfaces, but material was shed from high-standing intercrater plains to fill and bury craters lower in the landscape, then less densely cratered surfaces might have shallower craters.

[28] For craters >32 km in diameter through the widest craters in each unit, we found statistically significant differences at the 95% confidence level in both depth and diameter between the eNh and mNh units (Figure 5). Mean crater depth was 0.81 km for the eNh unit and 0.72 km for mNh. The mean diameters were 59 and 51 km, respectively. For both depth and diameter, a single-factor ANOVA rejected the null hypothesis that each sample is drawn from the same underlying probability distribution (p-value $= 1 \times 10^{-4}$ and 3×10^{-7}, respectively). This result suggests either that the crater size-frequency distribution changed between the Early and Middle Noachian Epochs, or that larger craters (particularly those over 90 km in diameter) were preferentially mapped into the eNh unit. *Tanaka et al.* (in review) dated impact craters and basins >150 km in diameter to place them into the correct geologic units, but smaller craters were not dated individually.

[29] We found no statistically significant relationship between depth and diameter for all craters or by unit (Figure 5d), due to their highly variable thicknesses of infill (such a relationship is expected for fresh craters, but it does not pertain to the degraded crater population). The greater mean depth of unit eNh craters may reflect slower infilling at their particular locations rather than their greater diameter.

[30] We also found no statistically significant difference in the depth/diameter ratios of craters between the eNh and mNh units at the 95% level (ANOVA p-value = 0.052) (Figure 5b). The mean depth/diameter ratio was 0.015 and 0.014 for the two units, respectively. A two-sample t-test assuming equal variances returned a one-tail $p(t < T)$ of 0.026, likely reflecting the greater number of very shallow craters in the mNh unit (Figure 5c). To identify the source of this result, we examined each unit mNh crater with a depth/diameter ratio <0.005. Negative values of depth and depth/diameter ratio were most commonly due to a degraded crater's location adjacent to a higher-relief crater, scarp, or slope, which introduced some low topographic points into the external surface elevation. Craters located on ridges or promontories, mostly surrounded by lower lying surfaces, can also have shallow depths in the *Robbins and Hynek* [2012a] data set. As expected, advanced crater degradation, embayment, and burial were important causes of shallow depth measurements between the crater floor and exterior surface, sometimes in combination with effects of the crater's topographic position. Figure 5a shows a histogram of depth/diameter ratios binned at intervals of 0.005, normalized to the number of craters in the eNh unit, as the mNh unit contained more craters >32 km in diameter due to its larger area.

[31] In summary, we found differences in both depth and diameter between the eNh and mNh units, although their mean depth/diameter ratios were similar. We found no evidence for the lower depth/diameter ratios that would be expected in the eNh unit if crater degradation were spatially and temporally uniform throughout the Noachian Period. However, we cannot exclude the possibility that some craters are preferentially infilled in the lower lying mNh unit. The results of this test reflect an integration of local

circumstances over the large area of the highlands, and the causes of crater infilling may vary from place to place, making a broad generalization on the cause of the depth and diameter relationships impossible without a much more detailed study of individual degraded craters.

3.3. Hypothesis 3: Spatial and Topographic Distribution

[32] Hypothesis 3 is that the spatial distribution of eNh, mNh, and lNh units is independent of topography. If this null hypothesis were true, then we would expect the eNh, mNh, and lNh units to occupy similar fractions of the total area in each elevation bin. Instead we find a complex relationship between area and elevation, where the fractional area of each unit varies substantially among several broad elevation ranges. This result falsifies the null hypothesis.

[33] When binning at 500 m intervals, Figure 6a shows that the mNh and lNh units share a modal elevation bin of 1000–1500 m, with their three most extensive bins within the 500–2000 m range. The modal elevation bin of eNh is 500 m higher. The extent of all three units falls off rapidly above 2000 m. Between −2000 and +500 m, the mNh unit has a broad shoulder that represents extensive outcrops in Arabia Terra, whereas the lNh and eNh units have much smaller distributions in this elevation range.

[34] Figure 6b shows the area of the eNh, mNh, and lNh units within each elevation bin, normalized to the total area of the three units within that bin. There is very little area in highland outcrops below −4000 m, so that elevation range is not shown. The broad rise in the fractional area of mNh is visible between −2000 and +500 m (mostly Arabia Terra). Between 500 and 3000 m, the fractional area of eNh increases at the expense of both mNh and lNh. The eNh unit occupies about half of the total area between 2000 and 3000 m elevations on the highland plateau. The mNh unit occupies more of the area between 3000 and 6500 m, which is mostly the Thaumasia range. Some of the highest-standing mountains in that area are also mapped as eNh, which dominates over a small area at elevations above 6500 m.

[35] The spatial distribution of the eNh and mNh units provides some insight into their origin (Figure 2). The eNh unit is primarily located within the high-standing Hellas ejecta annulus and in rugged surfaces of Terra Cimmeria and Terra Sirenum, coincident with areas of strong crustal magnetization [e.g., *Connerney et al*., 1999; *Lillis et al*., 2008]. This occurrence suggests that much of the unit is associated with the Hellas impact, but that some outcrops in Terra Cimmeria and Terra Sirenum may have a thin veneer of Hellas ejecta over older magnetized crust. The mNh unit is primarily found in Arabia Terra, within one inner ring diameter of the Argyre inner ring, and in lower lying areas between eNh outcrops on the highland plateau. Outcrops of unit lNh, on the other hand, are scattered throughout the highlands in local lows, indicative of localized highland infill.

3.4. Hypothesis 4: Proximity to Impact Basins

[36] A crater count on the Early Noachian highland massif (eNhm) unit, which is associated with Hellas basin, gave a slightly younger age than the eNh unit (Table 1), due to smaller densities in the unit eNhm 1–5.7 and 32–128 km diameter bins. The age of the eNhm unit is still above the *Hartmann* [2005] 4 Ga isochron line (Figure 4). These relative ages of units eNhm and eNh are consistent with resurfacing of unit eNh during the Hellas impact, as some unit eNh craters may be partly buried by Hellas ejecta, and some crater losses in the 32–128 km range were likely due to erosion and burial in the high-relief eNhm unit. Losses in the lower diameter range may be attributable to relief and to the middle latitude range that the unit occupies, where modification by ice and dust has been more effective than in equatorial areas [e.g., *Soderblom et al*., 1974; *Kreslavsky and Head*, 2000; *Stepinski et al*., 2009; *Robbins and Hynek*, 2012b].

[37] In the global geologic map, Isidis basin has proximal outcrops of the Middle Noachian highland massif unit (mNhm) surrounded mostly by units eNh and mNh in the region between the two main rings (Figure 2). *Frey* [2006], *Werner* [2008], *Fassett and Head* [2011], and *Robbins and Hynek* [2012c] all dated Isidis to near the Early/Middle Noachian boundary, which has a model absolute age of 3.96–3.97 Ga [*Werner and Tanaka*, 2011]. Our crater count gave a similar result on the Isidis massif unit, which is most directly linked to basin formation (Table 1 and Figure 4).

[38] The mNhm unit between the inner and outer rings of Argyre basin falls below the 4 Ga isochron and is consistent with later basin formation relative to Hellas (Figure 4). Three recent studies have also dated Argyre to the Middle Noachian Epoch, consistent with the results in the global geologic map and presented here [*Werner*, 2008; *Fassett and Head*, 2011; *Robbins and Hynek*, 2012c], although studies based on quasi-circular depressions (interpreted as possible buried craters) give it a relative age older than Isidis [*Frey*, 2006; *Roberts et al*., 2009]. Argyre has an inner basin diameter of only 900 km, so it should represent a less significant resurfacing of the highlands than Isidis (1500 km) and Hellas (2400 km). These studies [*Werner*, 2008; *Fassett and Head*, 2011; *Robbins and Hynek*, 2012c] along with *Schultz and Rogers* [1984] all place the sequence of impacts as Hellas first, then Isidis, and Argyre last. This sequence is also consistent with *Barlow*'s [1988] finding that most of the Martian intercrater plains, here represented by the mNh unit, formed between the Hellas and Argyre impacts (Table 1).

4. Discussion

[39] The hypothesis tests described above show that crater losses due to Noachian highland resurfacing were not spatially uniform, that reductions in crater depth/diameter ratios did not depend solely on unit age, and that highland surface ages vary with elevation and region. After the effects of impact basin resurfacing are recognized, these results show that crater infilling and burial were spatially variable in the highlands, and not just a function of time. The results also have implications for which geomorphic processes could be responsible.

[40] The Early Noachian surfaces in the Hellas ejecta annulus and its highland massif unit are consistent with the Early Noachian age of that basin, with progressively younger ages for Isidis and Argyre. Adequate time was available for the Hellas ejecta annulus to become nearly saturated with craters in the 32–128 km diameter range. Hellas ejecta thinly mantle the highlands of Terra Cimmeria and Terra Sirenum in the region of strong crustal magnetization

around 180° longitude, so this region may represent the pre-Hellas surface better than most regions of Mars.

[41] Highland resurfacing around a model absolute age of 4 Ga (possibly including a long span of time around that age) resulted in a loss of craters across a broad area of Mars, forming the mNh unit (Figures 2 and 3). Although this resurfacing occurred near the time of the Isidis impact (Table 1), it was much more extensive than the basin ejecta. Much of the mNh unit forms relatively low-lying surfaces between eNh outcrops, suggesting that erosion from local sources to sinks could be responsible. However, regionally extensive areas outside the Hellas annulus were also modified, including in Arabia Terra, suggesting that some areas of Mars experienced more complete resurfacing than others [*Hynek and Phillips*, 2001]. The Middle Noachian age of Argyre basin may explain some of the resurfacing in its vicinity. The distribution of the lNh unit is relatively straightforward, as it is primarily basin fill.

[42] Figures 3 and 4 show that the significant differences in crater densities between the eNh and mNh units are in the >32 km bins, whereas the <16 km bins have similar densities. This result suggests that the complete resurfacing of the mNh unit around a model absolute age of 4 Ga also eliminated most of the smaller craters in the eNh unit. Although the crater size-frequency distributions of these two units may reflect a distinct heavy-bombardment production population [e.g., *Strom et al*., 1992, 2005], locally to regionally complete resurfacing in the Middle Noachian is still required to explain the distinct ages of the units, and ubiquitous but incomplete resurfacing is needed to account for the similar densities of small craters and the observed crater degradation across all diameters in both units.

[43] Aside from basin ejecta, candidate resurfacing processes for the Noachian highlands include mass wasting (possibly facilitated by surface or ground ice), air fall mantling, burial by aeolian saltation deposits, fluvial or lacustrine deposition, and volcanism. The concentration of deeply buried areas (particularly lNh, but also mNh) with low relative ages in local lows in the landscape is consistent with a gravity-driven resurfacing process. It is inconsistent with air fall mantling on a global scale, which should be less topographically restricted to basin floors and should have more diffuse contacts. *Forsberg-Taylor et al*. [2004] also showed that air fall mantling does not explain degraded crater morphology in the equatorial region well. However, the more complete Middle Noachian resurfacing of Arabia Terra may have had an important aeolian component, and surface or subsurface water may have affected crater morphology and cemented surficial deposits [e.g., *Andrews-Hanna et al*., 2010, 2012; *Andrews-Hanna and Lewis*, 2011; *Barlow et al*., 2012]. Mass wasting is slope-dependent and generally does not form broad, flat plains. Volcanism has been an effective resurfacing process across much of the Martian highlands, and it may have been so during the Noachian Period as well [e.g., *Greeley and Spudis*, 1978]. However, it explains neither the progressive modification of crater rims and ejecta with time, nor the observed loss of craters on mNh surfaces, many of which are sloping, so other geomorphic processes are required. Aqueous weathering and transport are the most effective means to erode topographic highs, regrade slopes, and fill basins, but the poor dissection and watershed integration in the multibasin highlands point to arid-zone, transport-limited conditions [*Irwin et al*., 2011]. The relative importance of fluvial erosion, volcanism, and aeolian traction deposits in Noachian highland resurfacing cannot be distinguished with only the data used in this study. It is likely that all three processes along with disruption of fluvial pathways by concurrent impact cratering [*Irwin and Howard*, 2002; *Howard*, 2007] had important roles in the development of the mNh and lNh units, and that the relative effect of those processes varied from place to place.

5. Conclusions

[44] We tested four null hypotheses pertaining to Noachian highland resurfacing events and processes, using the new 1:20,000,000-scale global geologic map of Mars (*Tanaka et al*., in review), the crater data set of *Robbins and Hynek* [2012a, 2012b], and MOLA topography [*Smith et al*., 2001]. The hypotheses focused on the crater densities of mapped geologic units, the depth/diameter ratios of craters >32 km in diameter assigned to those units, the topographic distribution of the units, and the effect of resurfacing by impact basin ejecta. Impact craters from 1 to 4 km in diameter follow a mid-Hesperian *Hartmann* [2005] isochron, demonstrating a complete resurfacing of the highlands at that spatial scale since the Noachian. Craters in that size range are therefore not useful for dating Noachian surfaces. Noachian craters from 4 to 32 km in diameter experienced partial resurfacing losses that were inverse to diameter (the amount of crater loss in this diameter range depends strongly on whether there was a distinct heavy bombardment crater population [e.g., *Strom et al*., 1992, 2005]). We find that the three major highland units have distinct ages based on >32 km craters, so Noachian resurfacing was not spatially uniform. The eNh unit is concentrated in the Hellas basin annulus and in magnetized crust that was relatively thinly mantled by basin ejecta near 180° longitude. The unit is nearly saturated with craters of 32–128 km diameters. The mNh unit has a resurfacing age of ~4 Ga, similar to the age of Isidis basin, although its large areal extent requires effective resurfacing processes other than basin ejecta. Some of the resurfacing of mNh could involve erosion and deposition between local sources and sinks on the highland plateau, but its widespread occurrence across Arabia Terra requires a more regionally extensive resurfacing process in that area. The lNh unit includes younger composite surfaces of basin fill and partially buried cratered terrain, mostly confined to local lows. Following the Hellas impact, the cratered highlands experienced topographically controlled resurfacing, with lower lying areas experiencing more complete resurfacing on both regional (as shown here, exclusive of the uplifted Thaumasia range) and local scales (as observed during mapping).

[45] Although the highland units have statistically distinct crater densities and therefore ages, crater depth/diameter ratios do not vary strongly between the eNh and mNh units, suggesting that infilling of craters was not spatially and temporally uniform across Mars. Noachian resurfacing was long-lived, gravity-driven, and effective at both forming plains and modifying crater rims, which rules out uniform air fall mantling and mass wasting as dominant processes. Significant roles for arid-zone fluvial and aeolian erosion as well as volcanism are possible. However, reducing crater densities on mNh slopes between the high-standing eNh and

basin-infilling lNh units likely requires an erosional process rather than flood volcanism.

[46] **Acknowledgments.** This study was funded by grants from the NASA Planetary Geology and Geophysics Program (NNH10AN97I, U.S. Geological Survey, K. L. Tanaka, Principal Investigator) and Mars Data Analysis Program (NNX10AE64G, Planetary Science Institute, R. P. Irwin III, Principal Investigator). We are grateful to Nadine Barlow and Caleb Fassett for their detailed reviews. We also thank Colin Dundas, Alan Howard, and Bob Craddock for helpful discussions on technical details of the paper.

References

Andrews-Hanna, J. C., M. T. Zuber, R. E. Arvidson, and S. M. Wiseman (2010), Early Mars hydrology: Meridiani playa deposits and the sedimentary record of Arabia Terra, *J. Geophys. Res.*, *115*, E06002, doi:10.1029/2009JE003485.

Andrews-Hanna, J. C., and K. W. Lewis (2011), Early Mars hydrology: 2. Hydrological evolution in the Noachian and Hesperian epochs, *J. Geophys. Res.*, *116*, E02007, doi:10.1029/2010JE003709.

Arvidson, R. E. (1974), Morphologic classification of Martian craters and some implications, *Icarus*, *22*, 264–271.

Arvidson, R. E., et al. (2006), Overview of the Spirit Mars Exploration Rover Mission to Gusev crater: Landing site to Backstay Rock in the Columbia Hills, *J. Geophys. Res.*, *111*, E02S01, doi:10.1029/2005JE002499.

Barlow, N. G. (1988), Crater size-frequency distributions and a revised Martian relative chronology, *Icarus*, *75*, 285–305.

Barlow, N. G. (1990), Constraints on early events in Martian history as derived from the cratering record, *J. Geophys. Res.*, *95*, 14,191–14,201.

Barlow, N. G. (1995), The degradation of impact craters in Maja Valles and Arabia, Mars, *J. Geophys. Res.*, *100*(E11), 23,307–23,316, doi:10.1029/95JE02492.

Barlow, N. G., C. M. Atkins, M. E. Landis, and M. S. Talbot (2012), The influence of surface and subsurface volatiles in the evolution of Arabia Terra, Mars, *Third Conference on Early Mars*, Lunar Planet. Inst., Houston, Texas, abstract 7027.

Barnhart, C. J., A. D. Howard, and J. M. Moore (2009), Long-term precipitation and late-stage valley network formation: Landform simulations of Parana basin, Mars, *J. Geophys. Res.*, *114*, E01003, doi:10.1029/2008JE003122.

Berman, D. C., D. A. Crown, and L. F. Bleamaster III (2009), Degradation of mid-latitude craters on Mars, *Icarus*, *200*, 77–95.

Bouley, S., V. Ansan, N. Mangold, P. Masson, and G. Neukum (2009), Fluvial morphology of Naktong Vallis, Mars: A late activity with multiple processes, *Planet. Space Sci.*, *57*, 982–999, doi:10.1016/j.pss.2009.01.015.

Carr, M. H. (1995), The Martian drainage system and the origin of valley networks and fretted channels, *J. Geophys. Res.*, *100*(E4), 7479–7508, doi:10.1029/95JE00260.

Carr, M. H., and F. C. Chuang (1997), Martian drainage densities, *J. Geophys. Res.*, *102*(E4), 9145–9152, doi:10.1029/97JE00113.

Chapman, C. R., and K. L. Jones (1977), Cratering and obliteration history of Mars, *Annu. Rev. Earth Planet. Sci.*, *5*, 515–540.

Chapman, C., J. Pollack, and C. Sagan (1969), An analysis of the Mariner 4 cratering statistics, *Astron. J.*, *74*, 1039–1051.

Connerney, J. E. P., M. H. Acuña, P. J. Wasilewski, N. F. Ness, H. Rème, C. Mazelle, D. Vignes, R. P. Lin, D. L. Mitchell, and P. A. Cloutier (1999), Magnetic lineations in the ancient crust of Mars, *Science*, *284*, 794–798.

Craddock, R. A., and T. A. Maxwell (1993), Geomorphic evolution of the Martian highlands through ancient fluvial processes, *J. Geophys. Res.*, *98*, 3453–3468.

Craddock, R. A., T. A. Maxwell, and A. D. Howard (1997), Crater morphometry and modification in the Sinus Sabaeus and Margaritifer Sinus regions of Mars, *J. Geophys. Res.*, *102*, 13,321–13,340.

Crater Analysis Techniques Working Group (1979), Standard techniques for presentation and analysis of crater size-frequency data, *Icarus*, *37*, 467–474.

Edgett, K. S. (2005), The sedimentary rocks of Sinus Meridiani: Five key observations from data acquired by the Mars Global Surveyor and Mars Odyssey orbiters, *Mars*, *1*, 5–58, doi:10.1555/mars.2005.0002.

Fassett C. I., and J. W. Head III (2008a), Valley network-fed, open-basin lakes on Mars: Distribution and implications for Noachian surface and subsurface hydrology, *Icarus*, *198*, 37–56, doi:10.1016/j.icarus.2008.06.016.

Fassett, C. I., and J. W. Head III (2008b), The timing of Martian valley network activity: Constraints from buffered crater counting, *Icarus*, *195*, 61–89, doi:10.1016/j.icarus.2007.12.009.

Fassett, C. I., and J. W. Head III (2011), Sequence and timing of conditions on early Mars, *Icarus*, *211*(2), 1204–1214, doi:10.1016/j.icarus.2010.11.014.

Forsberg-Taylor, N. K., A. D. Howard, and R. A. Craddock (2004), Crater degradation in the Martian highlands: Morphometric analysis in the Sinus Sabaeus region and simulation modeling suggest fluvial processes, *J. Geophys. Res.*, *109*, E05002, doi:10.1029/2004JE002242.

Frey, H. V. (2006), Impact constraints on, and a chronology for, major events in early Mars history, *J. Geophys. Res.*, *111*, E08S91, doi:10.1029/2005JE002449.

Grant, J. A. (1987), The geomorphic evolution of eastern Margaritifer Sinus, Mars, *in* Advances in Planetary Geology, National Aeronautics and Space Administration Technical Memorandum *89871*, p. 1–268.

Grant, J. A., and P. H. Schultz (1993), Degradation of selected terrestrial and Martian impact craters, *J. Geophys. Res.*, *98*, 11,025−11,042.

Grant, J. A., and S. A. Wilson (2011), Late alluvial fan formation in southern Margaritifer Terra, Mars, *Geophys. Res. Lett.*, *38*, L08201, doi:10.1029/2011GL046844.

Greeley, R., and P. D. Spudis (1978), Volcanism in the cratered terrain hemisphere of Mars, *Geophys. Res. Lett.*, *5*(6), 453–455, doi:10.1029/GL005i006p00453.

Gulick, V. C., and V. R. Baker (1990), Origin and evolution of valleys on Martian volcanoes, *J. Geophys. Res.*, *95*, 14,325–14,344.

Hartmann, W. K. (1966), Martian cratering, *Icarus*, *5*, 565–576.

Hartmann, W. K. (2005), Martian cratering 8. Isochron refinement and the history of Martian geologic activity, *Icarus*, *174*, 294–320.

Hartmann, W. K., and G. Neukum (2001), Cratering chronology and the evolution of Mars, *Space Sci. Rev.*, *96*, 165–194.

Hoke, M. R. T., and B. M. Hynek (2009), Roaming zones of precipitation on ancient Mars as recorded in valley networks, *J. Geophys. Res.*, *114*, E08002, doi:10.1029/2008JE003247.

Howard, A. D. (2007), Simulating the development of Martian highland landscapes through the interaction of impact cratering, fluvial erosion, and variable hydrologic forcing, *Geomorphology*, *91*, 332–363, doi:10.1016/j.geomorph.2007.04.017.

Howard, A. D., J. M. Moore, and R. P. Irwin III (2005), An intense terminal epoch of widespread fluvial activity on early Mars: 1. Valley network incision and associated deposits, *J. Geophys. Res.*, *110*, D12S14, doi:10.1029/2005JE002459.

Hynek, B. M., and R. J. Phillips (2001), Evidence for extensive denudation of the Martian highlands, *Geology*, *29*(5), 407–410, doi:10.1130/0091-7613(2001)029 < 0407:EFEDOT > 2.0.CO;2.

Hynek, B. M., M. Beach, and M. R. T. Hoke (2010), Updated global map of Martian valley networks and implications for climate and hydrologic processes, *J. Geophys. Res.*, *115*, E09008, doi:10.1029/2009JE003548.

Irwin, R. P., III, and J. A. Grant (2013), Geologic map of MTM −15027, −20027, −25027 and −25032 quadrangles, Margaritifer Terra region of Mars: U.S. Geol. Survey Scientific Investigations Map, scale 1:1,000,000, in press.

Irwin, R. P., III, and A. D. Howard (2002), Drainage basin evolution in Noachian Terra Cimmeria, Mars, *J. Geophys. Res.*, *107*(E7), doi:10.1029/2001JE001818.

Irwin, R. P., III, A. D. Howard, R. A. Craddock, and J. M. Moore (2005), An intense terminal epoch of widespread fluvial activity on early Mars: 2. Increased runoff and paleolake development, *J. Geophys. Res.*, *110*, E12S15, doi:10.1029/2005JE002460.

Irwin, R. P., III, R. A. Craddock, A. D. Howard, and H. L. Flemming (2011), Topographic influences on development of Martian valley networks, *J. Geophys. Res.*, *116*, E02005, doi:10.1029/2010JE003620.

Ivanov, B. A. (2001), Mars/Moon cratering rate ratio estimates, *Space Sci. Rev.*, *96*, 87–104.

Jankowski, D. G., and S. W. Squyres (1992), The topography of impact craters in "softened" terrain on Mars, *Icarus*, *100*, 26–39.

Jankowski, D. G., and S. W. Squyres (1993), "Softened" impact craters on Mars: Implications for ground ice and the structure of the Martian regolith, *Icarus*, *106*, 365–379.

Kreslavsky, M. A., and J. W. Head (2000), Kilometer-scale roughness of Mars: Results from MOLA data analysis, *J. Geophys. Res.*, *105*, 26,695–26,711.

Lewis, K. W., O. Aharonson, J. P. Grotzinger, R. L. Kirk, A. S. McEwen, and T.-A. Suer (2008), Quasi-periodic bedding in the sedimentary rock record of Mars, *Science*, *322*, 1532–1535, doi:10.1126/science.1161870.

Lillis, R. J., H. V. Frey, M. Manga, D. L. Mitchell, R. P. Lin, M. H. Acuña, and S. W. Bougher (2008), An improved crustal magnetic field map of Mars from electron reflectometry: Highland volcano magmatic history and the end of the Martian dynamo, *Icarus*, *194*, 575–596, doi:10.1016/j.icarus.2007.09.032.

Malin, M. C. (1976), Nature and origin of intercrater plains on Mars, in Studies of the surface morphology of Mars, PhD dissertation, California Institute of Technology, Pasadena.

Mangold, N., C. Quantin, V. Ansan, C. Delacourt, and P. Allemand (2004), Evidence for precipitation on Mars from dendritic valleys in the Valles Marineris area, *Science*, *305*, 78–81.

Mangold, N., S. Adeli, S. Conway, V. Ansan, and B. Langlais (2012a), A chronology of early Mars climatic evolution from impact crater degradation, *J. Geophys. Res.*, *117*, E04003, doi:10.1029/2011JE004005.

Mangold, N., E.S. Kite, M.G. Kleinhans, H. Newsom, V. Ansan, E. Hauber, E. Kraal, C. Quantin, and K. Tanaka (2012b), The origin and timing of fluvial activity at Eberswalde crater, Mars, *Icarus*, *220*(2) 530–551. doi:10.1016/j.icarus.2012.05.026.

Mars Channel Working Group (1983), Channels and valleys on Mars, *Geol. Soc. Amer. Bull.*, *94*, 1035–1054.

Melosh, H. J. (1989), Impact cratering: A geologic process, 245 pp., Oxford Univ. Press, New York.

Neumann G. A., M. T. Zuber, M. A. Wieczorek, P. J. McGovern, F. G. Lemoine, and D. E. Smith (2004), Crustal structure of Mars from gravity and topography, *J. Geophys. Res.*, *109*, E08002, doi:10.1029/2004JE002262.

Oberbeck, V. R., W. L. Quaide, R. E. Arvidson, and H. R. Aggarwal (1977), Comparative studies of lunar, Martian, and Mercurian craters and plains, *J. Geophys. Res.*, *82*, 1681–1698.

Öpik, E. J. (1966), The Martian surface, *Science*, *153*, 255–265.

Pieri, D. C. (1980), Geomorphology of Martian valleys, in *Advances in Planetary Geology*, *NASA TM-81979*, pp. 1–160.

Robbins, S. J., and B. M. Hynek (2012a), A new global database of Mars impact craters ≥1 km: 1. Database creation, properties, and parameters, *J. Geophys. Res.*, *117*, E05004, doi:10.1029/2011JE003966.

Robbins, S. J., and B. M. Hynek (2012b), A new global database of Mars impact craters ≥1 km: 2. Global crater properties and regional variations of the simple-to-complex transition diameter, *J. Geophys. Res.*, *117*, E06001, doi:10.1029/2011JE003967.

Robbins, S. J., and B. M. Hynek (2012c), Revising the earliest recorded impact history of Mars and implications for the Late Heavy Bombardment, *Early Solar System Impact Bombardment 2*, Lunar Planet. Inst., Houston, Texas, Abstract 4039.

Roberts, J. H., R. J. Lillis, and M. Manga (2009), Giant impacts on early Mars and the cessation of the Martian dynamo, *J. Geophys. Res.*, *114*, E04009, doi:10.1029/2008JE003287.

Schultz, P. H., and J. Rogers (1984), Evolution of erosional styles of Martian impact basins, *15th Lunar Planet. Sci. Conf.*, Lunar Planet. Inst., Houston Texas, 734–735.

Smith, D. E., et al. (2001), Mars Orbiter Laser Altimeter: Experiment summary after the first year of global mapping of Mars, *J. Geophys. Res.*, *106*(E10), 23,689–23,722, doi:10.1029/2000JE001364.

Soderblom, L. A., C. D. Condit, R. A. West, B. M. Herman, and T J. Kreidler (1974), Martian planetwide crater distributions: Implications for geologic history and surface processes, *Icarus*, *22*, 239–263.

Stepinski, T. F., M. P. Mendenhall, and B. D. Bue (2009), Machine cataloging of impact craters on Mars, *Icarus*, *203*, 77–87, doi:10.1016/j.icarus.2009.04.026.

Strom, R. G., S. K. Croft, and N. D. Barlow (1992), The Martian impact cratering record, in Mars, edited by H. H. Kieffer et al., pp. 383–423, University of Arizona Press, Tucson.

Strom, R. G., R. Malhotra, T. Ito, F. Yoshida, and D. A. Kring (2005), The origin of planetary impactors in the inner solar system, *Science*, *309*, 1847–1850.

Tanaka, K. L. (1986), The stratigraphy of Mars, *J. Geophys. Res.*, *91*, E139–E158.

Tanaka, K. L., J. M. Dohm, C. M. Fortezzo, R. P. Irwin, E. J. Kolb, J. A. Skinner Jr., T. M. Hare, T. Platz, G. Michael, and S. Robbins (2012), The geology of Mars: What the new global map shows, *43rd Lunar Planet. Sci. Conf.*, Lunar Planet. Inst., Houston, Texas, Abstract 2702.

Werner, S. C. (2008), The early Martian evolution—Constraints from basin formation ages, *Icarus*, *195*, 45–60, doi:10.1016/j.icarus.2007.12.008.

Werner, S. C., and K. L. Tanaka (2011), Redefinition of the crater-density and absolute-age boundaries for the chronostratigraphic system of Mars, *Icarus*, *215*, 603–607, doi:10.1016/j.icarus.2011.07.024.